

Universal relations for anisotropic interacting quark stars

Juan M. Z. Pretel^{1,*} and Chen Zhang^{2,†}

¹*Centro Brasileiro de Pesquisas Físicas, Rua Dr. Xavier Sigaud,
150 URCA, Rio de Janeiro CEP 22290-180, RJ, Brazil*

²*The HKUST Jockey Club Institute for Advanced Study,
The Hong Kong University of Science and Technology, Hong Kong S.A.R., P.R.China*

(Dated: January 24, 2024)

Interacting quark stars, which are entirely composed of interacting quark matter including perturbative QCD corrections and color superconductivity, can meet constraints from various pulsar observations. In realistic scenarios, pressure anisotropies are expected in the star's interior. Recently, the stellar structural properties of anisotropic interacting quark stars have been investigated. In this study, we further explore the universal relations (URs) related to the moment of inertia I , tidal deformability Λ , compactness C , and the f -mode nonradial pulsation frequency for such stars. Our results reveal that these approximate URs generally hold, being insensitive to both the EOS variations as well as to the presence of anisotropy. Specifically, we find that more positive anisotropy tends to enhance the $I - \Lambda$ and $I - C$ URs, but weakens the $C - \Lambda$ UR. For all the URs involving f -mode frequency, we find that they are enhanced by the inclusion of anisotropy (whether positive or negative).

I. INTRODUCTION

Empirically, it is known that hadronic matter (HM) is bound at nuclear densities to form neutron stars (NSs). However, it is theoretically possible that compact stars are described by quark degrees of freedom, a matter phase called quark matter (QM), which can form bare quark stars (QSSs) that are highly compact.

The Bodmer-Witten-Terazawa hypothesis [1–3] suggests that QM with comparable amounts of u , d , s quarks, also called strange quark matter (SQM), might be the ground state of baryonic matter at low (zero) temperature and pressure. A recent study [4] demonstrated that u, d quark matter (ud QM) is, in general, more stable than SQM and the ordinary nuclear matter at a sufficiently large baryon number beyond the periodic table. Such bulk absolute stability allows the possibility of up-down quark stars consisting of ud QM [5–14], in addition to strange quark stars consisting of SQM [1–3, 15–23]. Interacting quark matter (IQM) includes the interquark effects induced by strong interaction, such as the perturbative QCD (pQCD) corrections [15, 24, 25] and the color superconductivity [26–28]. Recently, it was shown that the equation of state (EOS) of IQM can be recast into a simple unified form and the resulting interacting quark stars (IQSSs) can reconcile various astrophysical constraints [29], which has motivated a series of follow-up studies [30–37] using this IQM EOS. In a realistic scenario, anisotropy effects should also be accounted for in QSSs, which have been an active research area [38–48]. Very recently, anisotropic effects on the stellar structures of IQSSs have been systematically studied [49].

Anisotropy in compact stars can naturally arise from

various factors, such as large magnetic fields, phase transitions, relativistic nuclear interactions, crystallization or superfluidity of the core. Several models have been proposed to incorporate anisotropic pressure in compact stars, such as the Bowers-Liang (BL) model [50], Quasi-Local (QL) model [51], Herrera and Barreto (HB) model [52], etc. In general, the anisotropy may affect various macroscopic properties, such as mass, radius, moment of inertia, tidal deformability [49], radial [53] and nonradial oscillations [46, 54], with a large degeneracy on comparable effects from the EOS variations. It is thus physically important to investigate the effect of anisotropy in universal relations (URs) that are EOS insensitive.

The various URs between these quantities are insensitive to EOSs, and thus can be used to extract information from one to the others that may not be easy observables, and can help break the degeneracy in data analyses and model selections for various electromagnetic and GW observations. The URs for the moment of inertia (I), tidal deformability (Love), and spin-induced quadrupole moment (Q), were first derived by Yagi and Yunes for NSs that are slowly rotating, tidally deformed, isotropic [55, 56] or anisotropic [57], being generally hold both for NSs and QSSs [58–61]. There are also other URs involving star compactness (C) [59, 62, 63], and fundamental-mode frequency (f) of nonradial oscillations [64–67]. Recently, $I - \text{Love} - C$ and $I - f - C$ URs for anisotropic NSs were studied in Ref. [68] using BL model and Ref. [54] using QL model, and it was found that anisotropy will generally weaken the universal relations in BL model for the former, but will enhance or weaken the URs in QL model depending on the sign of anisotropy parameters for the latter. In this study, we generalize the exploration of these URs to anisotropic quark stars.

As for the organization of this paper, we first review the details of IQM. We then introduce the QL anisotropy

* juanzarate@cbpf.br

† iasczhang@ust.hk (Corresponding author)

profile, where a free parameter β_{QL} controls the amount of anisotropy within the IQS. After that, we apply this anisotropy model to the stellar properties of IQSs, such as the mass-radius, moment of inertia, tidal deformability, and nonradial oscillations under the Cowling approximation, with the main focus on their URs. All stellar structure equations will be rewritten in a dimensionless rescaled form so that the different macroscopic properties and the URs do not depend on the specific value of the effective bag constant B_{eff} . Finally, we discuss the sensitivity of these universal relations to the quark matter EOSs and anisotropy parameter variations. Throughout this work, we adopt the geometrized unit system where $G = 1 = c$.

II. MODELING OF ANISOTROPIC INTERACTING QUARK STARS

A. Equation of state for radial pressure

Our study involves anisotropic stellar fluids where in addition to a radial pressure p_r there is a transverse pressure p_t . Here we will begin by describing the equation of state for radial pressure. Referring to [29, 69], we first rewrite the thermodynamic potential Ω of interacting quark matter with the superconducting effect [70] and the pQCD correction included:

$$\Omega = -\frac{\xi_4}{4\pi^2}\mu^4 + \frac{\xi_4(1-a_4)}{4\pi^2}\mu^4 - \frac{\xi_{2a}\Delta^2 - \xi_{2b}m_s^2}{\pi^2}\mu^2 \quad (1)$$

$$- \frac{\mu_e^4}{12\pi^2} + B_{\text{eff}}, \quad (2)$$

where μ and μ_e are the respective average quark and electron chemical potentials. The first term represents the unpaired free quark gas contribution. The second term with $(1-a_4)$ represents the pQCD contribution from one-gluon exchange for gluon interaction to $O(\alpha_s^2)$ order. To phenomenologically account for higher-order contributions, we can vary a_4 from $a_4 = 1$, corresponding to a vanishing pQCD correction, to very small values where QCD corrections become large [21, 24, 69]. The term with m_s accounts for the correction from the finite strange quark mass if applicable. The term with the gap parameter Δ represents the contribution from color superconductivity. $(\xi_4, \xi_{2a}, \xi_{2b})$ represents different state of color-superconducting phases. Moreover, B_{eff} denotes the effective bag constant, accounting for the nonperturbative contribution from QCD vacuum.

The corresponding EOS for the radial pressure was derived in Ref. [29]:

$$p_r = \frac{1}{3}(\rho - 4B_{\text{eff}}) + \frac{4\lambda^2}{9\pi^2} \left[-1 + \text{sgn}(\lambda) \sqrt{1 + 3\pi^2 \frac{(\rho - B_{\text{eff}})}{\lambda^2}} \right], \quad (3)$$

where

$$\lambda = \frac{\xi_{2a}\Delta^2 - \xi_{2b}m_s^2}{\sqrt{\xi_4 a_4}}. \quad (4)$$

Note that $\text{sgn}(\lambda)$ represents the sign of λ . For this study, we need to explore only positive λ space, as preferred by astrophysical observations [29].

As shown in Ref. [29], one can further remove the B_{eff} parameter by doing the following dimensionless rescaling:

$$\tilde{\rho} = \frac{\rho}{4B_{\text{eff}}}, \quad \tilde{p}_r = \frac{p_r}{4B_{\text{eff}}}, \quad (5)$$

and

$$\tilde{\lambda} = \frac{\lambda^2}{4B_{\text{eff}}} = \frac{(\xi_{2a}\Delta^2 - \xi_{2b}m_s^2)^2}{4B_{\text{eff}}\xi_4 a_4}, \quad (6)$$

so that the EOS (3) reduces to the dimensionless form

$$\tilde{p}_r = \frac{1}{3}(\tilde{\rho} - 1) + \frac{4}{9\pi^2}\tilde{\lambda} \left[-1 + \sqrt{1 + \frac{3\pi^2}{\tilde{\lambda}}\left(\tilde{\rho} - \frac{1}{4}\right)} \right]. \quad (7)$$

As $\tilde{\lambda} \rightarrow 0$, Eq. (7) reduces to the rescaled conventional noninteracting quark matter EOS $\tilde{p}_r = (\tilde{\rho} - 1)/3$. On the other hand, when $\tilde{\lambda}$ becomes extremely large, Eq. (7) approaches the special form

$$\tilde{p}_r|_{\tilde{\lambda} \rightarrow \infty} = \tilde{\rho} - \frac{1}{2}, \quad (8)$$

or, equivalently, $p_r = \rho - 2B_{\text{eff}}$, using Eq. (5). We see that strong interaction effects can reduce the surface mass density of a quark star from $\rho_0 = 4B_{\text{eff}}$ down to $\rho_0 = 2B_{\text{eff}}$ and increase the quark matter radial sound speed $c_{rs}^2 = \partial p_r / \partial \rho$ from 1/3 up to 1 (the light speed) maximally.

B. Anisotropy profile

Anisotropic pressure in compact star systems may be a manifestation of several factors such as strong magnetic fields, phase transitions, pion condensation, rotation, bosonic composition, etc., see the review papers [71, 72] for further details. Consequently, anisotropic fluid configurations have been intensively analyzed in recent years using various ansatzes. The literature offers some functional relations for anisotropy, which must satisfy general physical requirements or “physical acceptability conditions” [73, 74]: 1) Energy density, radial pressure and tangential pressure should be positive anywhere within the anisotropic star, 2) gradients for energy density and radial pressure must be negative, 3) the radial and tangential speed of sound should be less than the speed of light, 4) the interior solution must satisfy the strong and dominant energy conditions, 5) regularity at the stellar center, among others. In our analysis, we will

adopt the phenomenological model that allows the construction of anisotropic stars obeying the aforementioned conditions. Originally introduced by Horvat and collaborators [51], the Quasi-Local ansatz is given by

$$\sigma = \beta_{\text{QL}} \left(\frac{2m(r)}{r} \right) p_r, \quad (9)$$

where β_{QL} is a dimensionless constant that measures the degree of anisotropy within the relativistic fluid sphere and $m(r)$ is the mass function. This profile has two important characteristics: First, it allows regularity at the stellar origin since the fluid becomes isotropic there, and second, because it arises only within a relativistic regime, i.e., its contribution is zero in the Newtonian limit. Its astrophysical implications on compact stars have been intensively investigated both in conventional Einstein gravity [46, 49, 53, 57, 75–78] and in modified gravity theories [79–83].

C. Mass-radius diagram

In Einstein gravity, the most basic properties of a compact star such as mass and radius are the results of numerically integrating the Tolman-Oppenheimer-Volkoff (TOV) equations [84, 85]:

$$\frac{dm}{dr} = 4\pi r^2 \rho, \quad (10)$$

$$\frac{dp_r}{dr} = (\rho + p_r) \frac{m + 4\pi r^3 p_r}{r(2m - r)} + \frac{2\sigma}{r}, \quad (11)$$

which are the product of considering an anisotropic perfect fluid described by the following energy-momentum tensor

$$T_{\mu\nu} = (\rho + p_t) u_\mu u_\nu + p_t g_{\mu\nu} - \sigma k_\mu k_\nu, \quad (12)$$

with ρ , p_r and p_t being the energy density, radial pressure and tangential pressure, respectively. Here, $\sigma = p_t - p_r$ is the anisotropic factor, k^μ is a unit spacelike four-vector and u^μ is the four-velocity of the fluid. The spacetime geometry of the stellar system is described by the metric

$$ds^2 = -e^{2\Phi(r)} dt^2 + e^{2\Psi(r)} dr^2 + r^2(d\theta^2 + \sin^2 \theta d\phi^2), \quad (13)$$

where $\Phi(r)$ and $\Psi(r)$ are the metric functions to be determined. The gravitational mass enclosed within a sphere of radius r , denoted by $m(r)$, is related to the metric function $\Psi(r)$ by means of $e^{-2\Psi(r)} = 1 - 2m(r)/r$. The surface radius R is calculated at which the radial pressure vanishes (i.e., by the condition $p_r(R) = 0$), and the total mass of the star is $M = m(R)$.

Meanwhile, the metric potential $\Phi(r)$ is obtained after solving the differential equation

$$\frac{d\Phi}{dr} = -\frac{1}{\rho + p_r} \frac{dp_r}{dr} + \frac{2\sigma}{r(\rho + p_r)}, \quad (14)$$

whose solution will be useful later when calculating other macroscopic properties of anisotropic IQSs. The boundary condition for (14) arises from the continuity of the interior metric (13) with the Schwarzschild exterior solution at the surface, namely

$$e^{2\Phi} = e^{-2\Psi} = 1 - \frac{2M}{R}. \quad (15)$$

Following the dimensionless rescaling (5), we have the rescaled variables for the anisotropy factor, radial coordinate and mass function as

$$\tilde{\sigma} = \frac{\sigma}{4B_{\text{eff}}}, \quad \tilde{r} = r\sqrt{4B_{\text{eff}}}, \quad \tilde{m} = m\sqrt{4B_{\text{eff}}}, \quad (16)$$

so the surface radius and total mass of the star will be denoted by \tilde{R} and \tilde{M} , respectively. The new dimensionless variables will be taken into account in all stellar structure equations such that the calculations are independent of the value of B_{eff} .

We begin our analysis by generating the rescaled mass-radius relations for several values of λ and β_{QL} . To this purpose, we numerically solve the system of equations (10) and (11) along with Eq. (9) by using the initial conditions $\rho(0) = \rho_c$ and $m(0) = 0$. Given a range of central densities, Fig. 1a displays the mass versus radius for anisotropic IQSs, where we have used five specific values of β_{QL} and the solid curves stand for the isotropic solutions when $\beta_{\text{QL}} = 0$. For the adopted anisotropy profile we have also considered three benchmark values of $\tilde{\lambda} = 0, 1$ and ∞ , where $\tilde{\lambda} = 0$ represents the standard noninteracting quark matter EOS. Remark that a larger $\tilde{\lambda}$ lead to more massive quark stars. It can be observed that positive (negative) anisotropies give rise to a substantial increase (decrease) in maximum-mass values of IQSs.

III. MOMENT OF INERTIA AND TIDAL DEFORMABILITY

Under the anisotropic context and in the slowly rotating approximation [86], the relativistic moment of inertia is calculated by first solving the following second-order differential equation [49]

$$\frac{e^{\Phi-\Psi}}{r^4} \frac{d}{dr} \left[e^{-(\Phi+\Psi)} r^4 \frac{d\varpi}{dr} \right] = 16\pi(\rho + p_r + \sigma)\varpi, \quad (17)$$

for the frame-dragging function $\varpi(r)$. This expression is integrated from the origin at $r = 0$ for an arbitrary choice of $\varpi(0)$ and with vanishing slope, i.e., $d\varpi/dr = 0$. Besides, the asymptotic flatness requirement has to be satisfied at very far distances from the stellar surface, so that $\lim_{r \rightarrow \infty} \varpi = \Omega$, where Ω is the angular velocity of the star. Thus, once the dragging angular velocity $\varpi(r)$ is found, the moment of inertia is determined via the integral

$$I = \frac{8\pi}{3} \int_0^R (\rho + p_r) \left[1 + \frac{\sigma}{\rho + p_r} \right] \frac{r^4 \varpi}{\Omega} e^{\Psi-\Phi} dr. \quad (18)$$

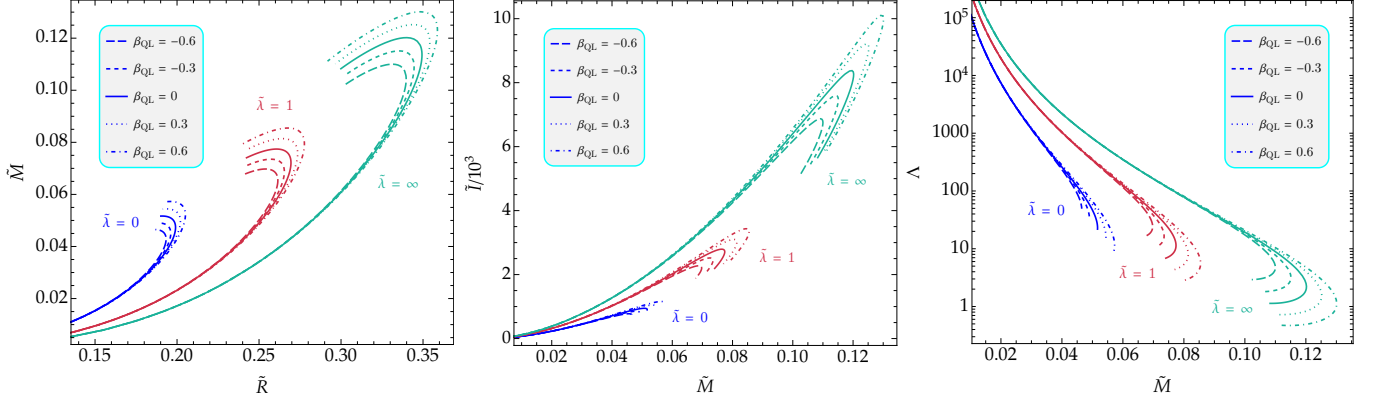


FIG. 1. From left to right, (a) Rescaled mass vs rescaled radius, (b) Dimensionless moment of inertia vs rescaled mass, and (c) Tidal deformability vs rescaled mass for anisotropic IQSs with $\tilde{\lambda} = 0, 1$ and ∞ for the interacting quark matter EOS (7) with QL anisotropy ansatz (9), where we have considered $\beta_{\text{QL}} \in [-0.6, 0.6]$.

It is important to emphasize that the frame-dragging function and moment of inertia in their dimensionless rescaled forms are given by

$$\tilde{\omega} = \frac{\varpi}{\sqrt{4B_{\text{eff}}}}, \quad \tilde{I} = I \sqrt{(4B_{\text{eff}})^3}. \quad (19)$$

For each value of central energy density ρ_c and given the anisotropy model (9), Eq. (17) along with the TOV equations are simultaneously solved. Our results for the integral (18) are illustrated in Fig. 1b, where we present the dimensionless moment of inertia \tilde{I} as a function of the total gravitational mass \tilde{M} . As the strong interaction effects become increasingly larger (i.e., as $\tilde{\lambda}$ increases), the moment of inertia is subjected to a relevant increase with respect to the non-interacting case. We further observe that the maximum values of \tilde{I} increase as β_{QL} increases from negative values.

The tidal perturbation $y(r)$ for the spacetime metric of the anisotropic star is governed by the equation [46]

$$ry' = -y^2 + (1 - r\mathcal{A})y - r^2\mathcal{B}, \quad (20)$$

where

$$\mathcal{A} = \frac{2}{r} + e^{2\Psi} \left[\frac{2m}{r^2} + 4\pi r(p_r - \rho) \right], \quad (21)$$

$$\begin{aligned} \mathcal{B} = & 4\pi e^{2\Psi} \left[4\rho + 4p_r + 4p_t + \frac{\rho + p_r}{\mathcal{F}v_{sr}^2} (1 + v_{sr}^2) \right] \\ & - \frac{6e^{2\Psi}}{r^2} - 4\Phi'^2, \end{aligned} \quad (22)$$

with $\mathcal{F} = dp_t/dp_r$ and $v_{sr}^2 = dp_r/d\rho$. Through the initial condition $y(0) = 2$ [87] at the center, we determine the surface tidal perturbation $y(R)$ by integrating the differential equation (20) from the origin up to the surface of the anisotropic interacting quark star. The dimensionless tidal deformability is given by $\Lambda = 2k_2/3C^5$, where $C = M/R$ is the compactness and tidal Love number k_2

has the form [46, 88]:

$$\begin{aligned} k_2 = & \frac{8}{5}(1 - 2C)^2 C^5 [2C(\alpha - 1) - \alpha + 2] \\ & \times \{2C[4(\alpha + 1)C^4 + (6\alpha - 4)C^3 \\ & + (26 - 22\alpha)C^2 + 3(5\alpha - 8)C - 3\alpha + 6] \\ & + 3(1 - 2C)^2 [2C(\alpha - 1) - \alpha + 2] \ln(1 - 2C)\}^{-1}. \end{aligned} \quad (23)$$

Note that, for compact stars with a nonzero density at the surface, $\alpha = y(R) - 4\pi R^3 \rho_s/M$ in the last expression, where ρ_s is the density just inside the stellar surface. Furthermore, the rescaling quantities for the new variables introduced take the form

$$\tilde{\mathcal{A}} = \frac{\mathcal{A}}{\sqrt{4B_{\text{eff}}}}, \quad \tilde{\mathcal{B}} = \frac{\mathcal{B}}{4B_{\text{eff}}}. \quad (24)$$

Equation (20) must be integrated self consistently with the TOV equations (10), (11) and (14) from the center of the star, where $\rho(0) = \rho_c$, to its surface at $r = R$. Fig. 1c exhibits the dimensionless tidal deformability as a function of total mass for the adopted anisotropy model. We observe that Λ becomes large for anisotropic IQSs near the minimum-mass configuration. Given a fixed value of \tilde{M} in the small-mass region, an increase in $\tilde{\lambda}$ leads to obtaining larger tidal deformabilities with respect to the non-interacting case.

It has been shown that the global properties of a compact star (such as mass, moment of inertia and tidal deformability) are connected by universal relations [56, 58, 59, 63, 89]. Under this perspective, in the present work we intend to analyze these universalities in the context of IQSs under the presence of anisotropic pressure. We begin by analyzing the $I - \Lambda$ relation through the normalized moment of inertia $\bar{I} = \tilde{I}/\tilde{M}^3$ [89]. Given a specific anisotropy model, \bar{I} is plotted as a function of the dimensionless tidal deformability Λ , see Fig. 2a for the QL ansatz where we have considered three benchmark

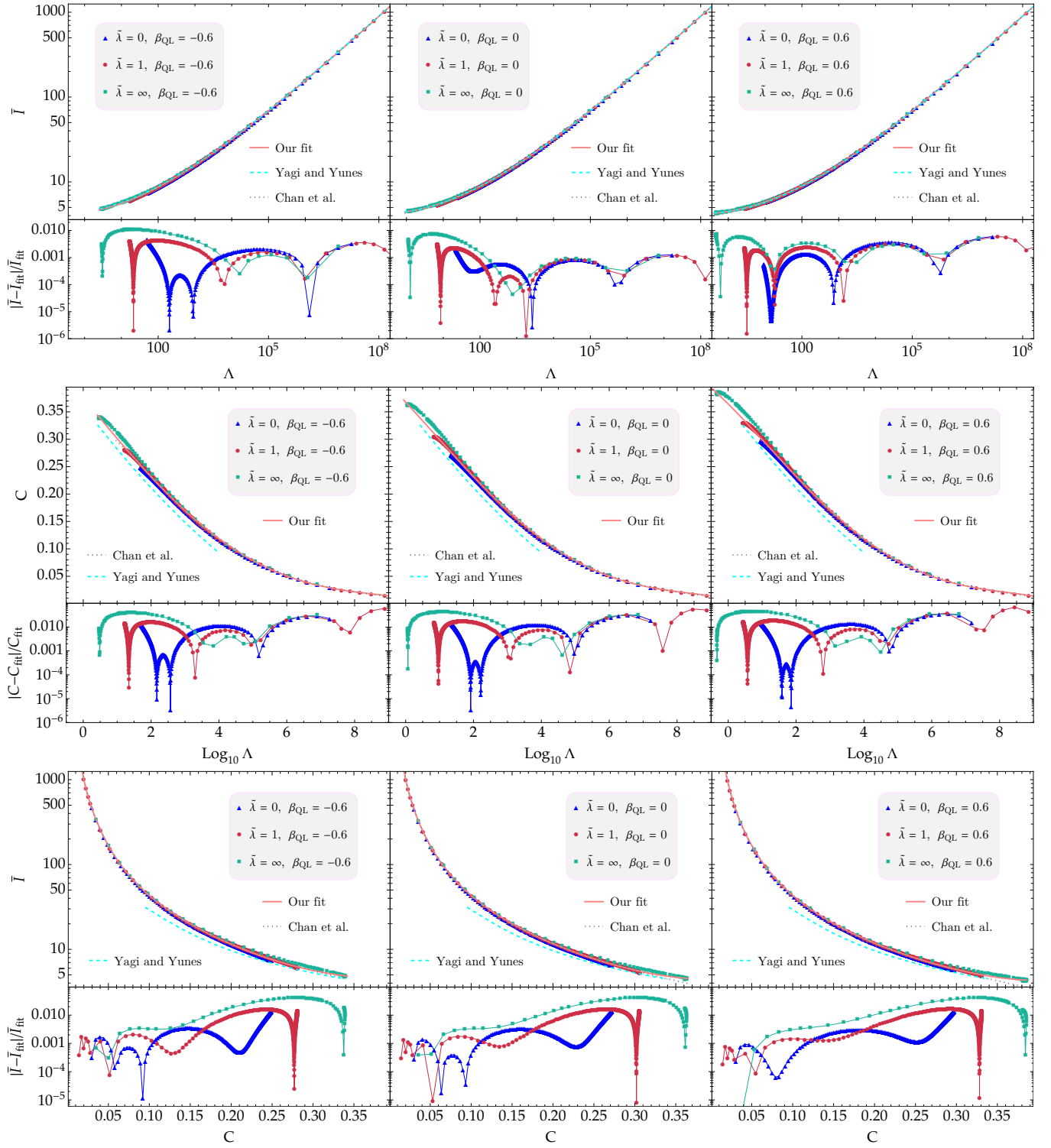


FIG. 2. From top to bottom, (a) $\bar{I} - \Lambda$, (b) $C - \Lambda$ and (c) $\bar{I} - C$ universal relations for anisotropic IQSs with the QL anisotropy ansatz (9), where we have assumed three benchmark values of $\beta_{\text{QL}} = -0.6$ (left column), 0 (middle column corresponding to the isotropic scenario) and 0.6 (right column). Different symbols indicate the respective EOS for the radial pressure with three benchmark values of $\tilde{\lambda}$. Pink solid lines represent our fitted curves using the series expansions (25), (26) and (27) of corresponding URs, with the lower panel in each plot displays the relative fractional errors between fits and the numerical results. Additionally, the gray dotted lines are the fitting functions for QSs derived within the post-Minkowskian approximation [59], while the cyan dashed curves are the analytical expressions for NSs [58].

values of β_{QL} . We fit these relations with the following power series expansion

$$\log_{10} \bar{I} = \sum_{n=0}^4 a_n (\log_{10} \Lambda)^n, \quad (25)$$

where a_n are fitting coefficients with their respective reduced chi-squared (χ_{red}^2) values listed in Table I. We can note that an increase in anisotropy (e.g., $\beta_{\text{QL}} = 0.6$) gives rise to a decrease in χ_{red}^2 value with respect to the isotropic case, which indicates that the EOS-insensitive UR of $\bar{I} - \Lambda$ gets enhanced with the addition of positive anisotropy, while the opposite occurs for negative anisotropies.

The lower panels in Fig. 2a display the absolute fractional difference between all numerical data (extracted by considering different EOSs with $\tilde{\lambda} = 0, 1, \infty$) and the fitting expression (25). It can be observed that, given a particular value of β_{QL} , the $\bar{I} - \Lambda$ relation remains approximately universal with maximum deviations at $\sim 1\%$ level in the range of adopted $\tilde{\lambda}$, which is constrained by different observational measurements [29, 49]. Thus, this relation is insensitive to the EOS of interacting quark stars even if there is anisotropic pressure (see the left and right plots for $\beta_{\text{QL}} \neq 0$) within the stellar fluid. Through a post-Minkowskian expansion for incompressible stars, Chan et al. [63] found analytic expressions for \bar{I} and Λ to sixth-order in compactness. A year later, the same authors extended this analysis to self-bound stars, which include quark stars, and they showed that the $\bar{I} - \Lambda$ relation is very similar to that for incompressible stars [59]. In Fig. 2a, we have included the fit obtained by Chan and collaborators [59] for the case of QSs by a gray dotted line. For comparison, we have also included the fitted curve for NSs obtained by Yagi and Yunes [58] by a cyan dashed line. We observe that the $\bar{I} - \Lambda$ correlation of NSs is almost indistinguishable from that of IQSs. We can therefore say that our \bar{I} – Love results are consistent with the analyses for other dense-matter EOSs. Furthermore, in Fig. 3a we provide the $\bar{I} - \Lambda$ UR when the anisotropy parameter varies in the range $|\beta_{\text{QL}}| \leq 0.6$ but $\tilde{\lambda}$ remains fixed to a benchmark value $\tilde{\lambda} = 1$. In this case, the $\bar{I} - \Lambda$ relation remains approximately universal with maximum deviations at the 3% level.

Fig. 2b displays the $C - \Lambda$ UR for the three EOSs, where each plot from left to right corresponds to a fixed value of β_{QL} as in Fig. 2a. A fit function of the form

$$C = \sum_{n=0}^4 b_n (\log_{10} \Lambda)^n \quad (26)$$

is also included in each plot by a pink curve. The best-fit coefficients are given in Table II. Contrary to what happened with the $\bar{I} - \Lambda$ correlation, here we see that positive anisotropies increase the value of χ_{red}^2 which weakens the $C - \Lambda$ EOS independent relation. Nevertheless, negative anisotropies make this UR stronger. We have included the fits obtained for NSs [58] and QSs [59] by cyan dashed

TABLE I. Fitting coefficients of the $\bar{I} - \Lambda$ UR given by the series expansion (25), with the anisotropy model (9) for three benchmark values of the anisotropy parameter β_{QL} . Moreover, the reduced chi-squared (χ_{red}^2) values are shown for all cases in the last row.

β_{QL}	-0.6	0	0.6
$a_0[10^{-1}]$	6.4232	6.4749	6.5096
$a_1[10^{-2}]$	5.2637	6.2737	7.0025
$a_2[10^{-2}]$	5.6645	5.0556	4.5931
$a_3[10^{-3}]$	-4.6588	-3.5984	-2.7527
$a_4[10^{-4}]$	1.5807	1.0003	0.5178
$\chi_{\text{red}}^2[10^{-6}]$	1.7645	0.5813	0.5612

TABLE II. Fitting coefficients of the $C - \Lambda$ UR given by the series expansion (26), with the same values of β_{QL} as in Table I. The respective values of χ_{red}^2 are given in the last row.

β_{QL}	-0.6	0	0.6
$b_0[10^{-1}]$	3.7539	3.6766	3.6448
$b_1[10^{-2}]$	-7.4469	-6.6742	-6.1748
$b_2[10^{-3}]$	-0.3753	-2.9372	-4.9372
$b_3[10^{-3}]$	0.9488	1.2898	1.5839
$b_4[10^{-5}]$	-5.3656	-6.9389	-8.3793
$\chi_{\text{red}}^2[10^{-5}]$	0.7736	1.0498	1.3769

TABLE III. Fitting parameters of the $\bar{I} - C$ UR given by the series expansion (27), with the same values of β_{QL} as in Table I. The respective values of χ_{red}^2 are given in the last row.

β_{QL}	-0.6	0	0.6
$c_{-4}[10^{-7}]$	-1.3945	-1.0597	-0.6584
$c_{-3}[10^{-5}]$	2.8396	2.1490	1.3560
$c_{-2}[10^{-3}]$	-2.2886	-1.7453	-1.1512
$c_{-1}[10^{-2}]$	0.1036	8.2858	6.1387
c_0	0.8531	1.2671	1.6668
c_1	0.9939	-3.3393	-7.2093
$c_2[10^1]$	-1.9843	0.3404	2.2466
$c_3[10^1]$	4.8042	-0.9847	-5.2987
$c_4[10^1]$	-2.8670	2.3648	5.8645
$\chi_{\text{red}}^2[10^{-5}]$	7.8028	6.9737	5.9877

and gray dotted lines, respectively. Our results reveal that the $C - \Lambda$ correlation of neutron stars is appreciably distinguishable from that of quark stars. However, our findings are compatible with the fit obtained by Chan et al. [59]. According to the bottom panels, the fractional difference between the data and the fit (26) show that the $C - \Lambda$ relation is approximately universal with maximum deviations at $\sim 8\%$ level, which is much larger than that of the $\bar{I} - \Lambda$ UR in Fig. 2a, whose maximum equation-of-state variation led to fractional errors of the order of 1%. From Fig. 3b, we observe also that this relation is insensitive to the variation of β_{QL} to $\sim 10\%$ level for fixed $\tilde{\lambda} = 1$.

Fig. 2c exhibits the relation between \bar{I} and C , for which our fit (pink curve) is built based on the following poly-

nomial function

$$\log_{10} \bar{I} = \sum_{n=-4}^4 c_n C^n, \quad (27)$$

where the fitting parameters c_n with their corresponding chi-squared (χ^2_{red}) errors are presented in Table III. Our results reveal that positive (negative) values of β_{QL} lead to a stronger (weaker) EOS insensitive $\bar{I} - C$ relation. Furthermore, according to the lower panels in Fig. 2c, the maximum fractional difference for the compact stars sequence is at least 5%, less than that of the $C - \Lambda$ UR but still much greater than that obtained in the $\bar{I} - \Lambda$ correlation. Remarkably, the $\bar{I} - C$ relation of IQSs is quite different from that of neutron-star matter (see the cyan dashed curve). Nonetheless, our fitting formula is consistent with the analytic expression for quark stars derived by Chan et al. [59], as shown by the gray dotted line. Moreover, Fig. 3c shows the $\bar{I} - C$ UR for fixed $\tilde{\lambda} = 1$, which is insensitive to variations of β_{QL} with maximum deviations at the 4% level. Therefore, the different URs analyzed so far remain insensitive not only to variations in the EOS of IQM but also to the presence of anisotropy (when $\beta_{\text{QL}} \neq 0$).

IV. NONRADIAL OSCILLATIONS

In addition to the URs already discussed above, it is also possible to provide empirical functions that do not depend on the specific EOS by involving the f -mode pulsation frequency [64–67]. Such a mode is the lowest-order, fundamental, nonradial oscillation mode, characterized by a zero node number. This work also aims to study the correlation between the dimensionless frequency $\Omega_f = \tilde{M}\tilde{\omega}_f$ and other macroscopic properties of IQSs within an anisotropic context. The impact of anisotropic pressure on the f -mode frequency of compact stars using hadronic matter [54, 78] and quark matter [46, 78] has been recently investigated. In the case of QSSs, the authors used the standard noninteracting quark matter EOS, i.e., the phenomenological MIT bag model EOS. We will extend such study considering strong interaction effects in dense matter of the compact star system. To do so, we will obtain the differential equations that govern the nonradial oscillations of anisotropic compact stars in the Cowling approximation for any anisotropy profile σ , as well as analyze in detail the different URs associated with the f -mode frequency. With this in mind, we start with the conservation equation for the energy-momentum tensor (12), namely

$$\nabla_\mu T^{\mu\nu} = [(\nabla_\mu \rho) u^\mu + (\rho + p_t)(\nabla_\mu u^\mu)] u^\nu + h^{\mu\nu} \nabla_\mu p_t + (\rho + p_t)a^\nu - \nabla_\mu(\sigma k^\mu k^\nu) = 0, \quad (28)$$

where $a^\mu = u^\nu \nabla_\nu u^\mu$ is the the four-acceleration of the fluid in the background metric and $h^{\mu\nu} = g^{\mu\nu} + u^\mu u^\nu$ is the projection tensor, which projects any tensor on the

hypersurface orthogonal to u_μ [90]. The nonradial oscillations equations are obtained by varying (28). Under the Cowling approximation [91], where the metric perturbations are neglected (namely, $\delta g^{\mu\nu} = 0$), the perturbation of the conservation equation $\delta(\nabla_\mu T^{\mu\nu}) = 0$ implies that

$$\begin{aligned} & [(\delta u^\mu) \nabla_\mu \rho + u^\mu \nabla_\mu \delta \rho + (\delta \rho + \delta p_t)(\nabla_\mu u^\mu) \\ & + (\rho + p_t)(\nabla_\mu \delta u^\mu)] u^\nu + [u^\mu \nabla_\mu \rho + (\rho + p_t)(\nabla_\mu u^\mu)] \delta u^\nu \\ & + (\nabla_\mu \delta p_t) u^\mu u^\nu + (\rho + p_t) [(\delta u^\mu) \nabla_\mu u^\nu + u^\mu \nabla_\mu \delta u^\nu] \\ & + g^{\mu\nu} \nabla_\mu \delta p_t + (\delta u^\mu) u^\nu \nabla_\mu p_t + u^\mu (\delta u^\nu) \nabla_\mu p_t \\ & + (\delta \rho + \delta p_t) a^\nu - \nabla_\mu \delta(\sigma k^\mu k^\nu) = 0, \end{aligned} \quad (29)$$

so that the projection of Eq. (29) along the four-velocity, i.e., $u_\nu \nabla_\mu(\delta T^{\mu\nu}) = 0$, leads to

$$\begin{aligned} & u^\mu \nabla_\mu \delta \rho + \nabla_\mu [(\rho + p_t) \delta u^\mu] + (\rho + p_t)(\delta u^\nu) a_\nu \\ & + u_\nu \nabla_\mu \delta(\sigma k^\mu k^\nu) = 0, \end{aligned} \quad (30)$$

where we have used the normalization condition $u_\mu u^\mu = -1$ and the orthogonality condition $u_\mu a^\mu = 0$. Notice that using the property $u_\mu k^\mu = 0$, Eq. (30) can be written in the form given as in Ref. [75]. Furthermore, projecting Eq. (29) in the space orthogonal to the four-velocity, i.e., $h^\alpha_\nu \nabla_\mu(\delta T^{\mu\nu}) = 0$, we find

$$\begin{aligned} & (\delta \rho + \delta p_t) a^\alpha + h^{\alpha\mu} \nabla_\mu \delta p_t + (\rho + p_t)(\delta u^\mu) \nabla_\mu u^\alpha \\ & + (\rho + p_t) u^\mu \nabla_\mu \delta u^\alpha - (\rho + p_t) u^\alpha (\delta u^\nu) a_\nu \\ & - h^\alpha_\nu \nabla_\mu \delta(\sigma k^\mu k^\nu) = 0. \end{aligned} \quad (31)$$

Fluid perturbation vectors inside a compact star can be decomposed in a basis of spherical harmonics. Thus, writing the Lagrangian displacement vector as [46]

$$\xi^i = \left(e^{-\Psi} W, -V \partial_\theta, -\frac{V}{\sin^2 \theta} \partial_\phi \right) \frac{Y_{\ell m}}{r^2}, \quad (32)$$

the explicit expression for the Eulerian variation of the four-velocity vector is given by

$$\delta u^\mu = \left(0, e^{-\Psi} \partial_t W, -\partial_t V \partial_\theta, -\frac{\partial_t V}{\sin^2 \theta} \partial_\phi \right) \frac{e^{-\Phi} Y_{\ell m}}{r^2}, \quad (33)$$

where $W = W(t, r)$ and $V = V(t, r)$ are fluid perturbation functions which depend on the time and radial coordinate, and $Y_{\ell m} = Y_{\ell m}(\theta, \phi)$ are the standard spherical harmonics. Taking into account the non-null components $k^1 = e^{-\Psi}$ and $\delta k^0 = e^{-2\Phi} \partial_t W Y_{\ell m}/r^2$, Eq. (30) provides the perturbation for energy density:

$$\begin{aligned} \delta \rho = & -(\rho + p_r) \left[\frac{e^{-\Psi}}{r^2} W' + \frac{\ell(\ell+1)}{r^2} V \right] Y_{\ell m} \\ & - \rho' \frac{e^{-\Psi}}{r^2} W Y_{\ell m} - 2\sigma \frac{e^{-\Psi}}{r^3} W Y_{\ell m} \\ & - \sigma \frac{\ell(\ell+1)}{r^2} V Y_{\ell m}, \end{aligned} \quad (34)$$

where the prime indicates derivative with respect to r .

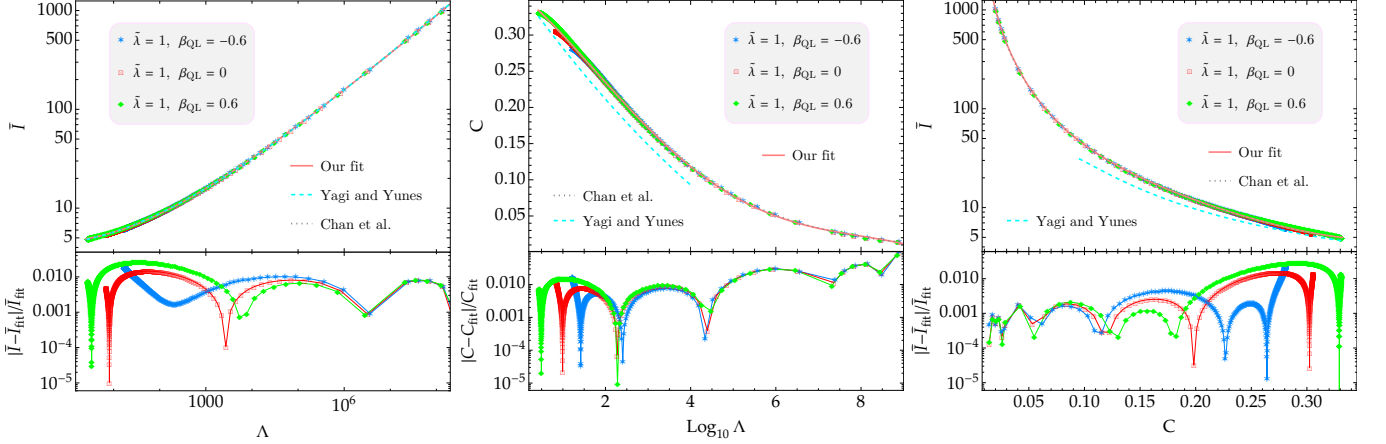


FIG. 3. From left to right, (a) $\bar{I} - \Lambda$, (b) $C - \Lambda$ and (c) $\bar{I} - C$ URs for anisotropic IQSs of a benchmark EOS choice $\tilde{\lambda} = 1$, with the QL anisotropy parameter varying in the range $|\beta_{\text{QL}}| \leq 0.6$. Pink solid lines represent our fitted curves, with the lower panel in each plot showing the relative fractional errors between fits and the numerical results. According to the relative fractional errors, these correlations remain approximately universal to 3%, 10% and 4% under variations of β_{QL} , respectively. The results for other $\tilde{\lambda}$ choices share similar features.

We assume a harmonic time dependence for the perturbation functions, namely $W(t, r) = W(r)e^{i\omega t}$, $V(t, r) = V(r)e^{i\omega t}$ and $\delta F(t, r, \theta, \phi) = \delta F(r)e^{i\omega t}Y_{\ell m}$, where F represents any fluid variable and ω is the nonradial oscillation frequency to be determined. Consequently, the $\alpha = 1$ component of Eq. (31) implies that

$$(\delta\rho + \delta p_r)\Phi' + (\delta p_r)' - \omega^2(\rho + p_r)\frac{e^{\Psi-2\Phi}}{r^2}W - \frac{2}{r}\delta\sigma = 0, \quad (35)$$

while for the index $\alpha = 2$, we obtain

$$\delta p_r + \delta\sigma + \omega^2(\rho + p_r + \sigma)e^{-2\Phi}V = 0. \quad (36)$$

In view of Eqs. (34)-(36) and taking into consideration that $\delta p_r = (dp_r/d\rho)\delta\rho$ due to the EOS $p_r = p_r(\rho)$, the nonradial perturbations of an anisotropic compact star in the Cowling approximation are described by

$$W' = \frac{d\rho}{dp_r} \left[(1+X)\omega^2 r^2 e^{\Psi-2\Phi}V + \Phi'W + \frac{r^2 e^\Psi \delta\sigma}{\rho + p_r} \right] - \left(1 + \frac{d\rho}{dp_r} \right) \frac{2}{r} XW - \ell(\ell+1)(1+X)e^\Psi V, \quad (37)$$

$$V' = \left[-\frac{\sigma'}{(\rho + p_r)(1+X)} + 2\Phi' - \left(1 + \frac{d\rho}{dp_r} \right) \left(\Phi' + \frac{2}{r} \right) \frac{X}{1+X} \right] V - \left(1 + \frac{d\rho}{dp_r} \right) \frac{e^{2\Phi} \Phi' \delta\sigma}{\omega^2(\rho + p_r)(1+X)} - \frac{e^\Psi}{r^2} \frac{W}{1+X} - \frac{e^{2\Phi}}{\omega^2(\rho + p_r)(1+X)} \left[\frac{2}{r} \delta\sigma + (\delta\sigma)' \right], \quad (38)$$

with $X = \sigma/(\rho + p_r)$. It is important to remark that this system of differential equations is valid for any anisotropy profile $\sigma(r)$. In particular, when the anisotropy vanishes (i.e., the quantities σ , X and $\delta\sigma$ are zero) we recover the equations corresponding to isotropic stars [92]. In addition, for the anisotropy model (9), that is, $\sigma = \beta_{\text{QL}}\mu p_r$, we have $\delta\sigma = (\partial\sigma/\partial p_r)\delta p_r$. This is because the variation $\delta\mu$ is associated with the variation of the metric potential Ψ , which is zero in the Cowling approximation. In this case, the perturbation for the anisotropy factor can be

written as

$$\delta\sigma = -\frac{\partial\sigma}{\partial p_r} \left(1 + \frac{\partial\sigma}{\partial p_r} \right)^{-1} \omega^2(\rho + p_r)(1+X)e^{-2\Phi}V. \quad (39)$$

By substituting Eq. (39) into the general system of time-independent differential equations (37) and (38), we hence manage to retrieve the nonradial oscillation equa-

tions for the QL model, namely [46]

$$\begin{aligned} W' = & \frac{d\rho}{dp_r} \left[(1+X) \left(1 + \frac{\partial\sigma}{\partial p_r} \right)^{-1} \frac{\omega^2 r^2 V}{e^{2\Phi-\Psi}} + \Phi' W \right] \\ & - X \left[\left(1 + \frac{d\rho}{dp_r} \right) \frac{2W}{r} + \ell(\ell+1)e^\Psi V \right] \\ & - \ell(\ell+1)e^\Psi V, \end{aligned} \quad (40)$$

$$\begin{aligned} V' = & V \left[-\frac{\sigma'}{\rho+p_r+\sigma} - \left(1 + \frac{d\rho}{dp_r} \right) \left(\Phi' + \frac{2}{r} \right) \frac{X}{1+X} \right. \\ & \left. + \frac{2}{r} \frac{\partial\sigma}{\partial p_r} + \left(1 + \frac{\partial\sigma}{\partial p_r} \right)^{-1} \left(\frac{\partial^2\sigma}{\partial p_r^2} p'_r + \frac{\partial^2\sigma}{\partial\mu\partial p_r} \mu' \right) \right] \\ & + 2\Phi' V - \left(1 + \frac{\partial\sigma}{\partial p_r} \right) \frac{e^\Psi W}{r^2(1+X)}. \end{aligned} \quad (41)$$

The above equations (40) and (41) will be solved numerically from the center up to the stellar surface of the anisotropic sphere. For this purpose, suitable boundary conditions have to be established. Thus, at $r=0$, we assume that the radial variables W and V take the respective forms

$$W = cr^{\ell+1}, \quad V = -c \frac{r^\ell}{\ell}, \quad (42)$$

where c stands for a dimensionless constant. Meanwhile, at $r=R$, the following condition has to be satisfied

$$(1+X) \frac{\omega^2 V}{e^{2\Phi}} + \left[1 + \frac{\partial\sigma}{\partial p_r} \right] \left[\frac{r\Phi'}{2} - X \right] \frac{2W}{e^\Psi r^3} = 0, \quad (43)$$

and in our calculations we will deal with the quadrupolar modes, that is, when $\ell=2$. Note further that the dimensionless rescaled form for the new variables involved in the nonradial perturbations is given by

$$\tilde{\omega} = \frac{\omega}{\sqrt{4B_{\text{eff}}}}, \quad \tilde{W} = (4B_{\text{eff}})^{3/2} W, \quad \tilde{V} = (4B_{\text{eff}}) V. \quad (44)$$

Chan et al. [65] found EOS-insensitive empirical formulas which relate the f -mode frequency and the tidal deformability of compact stars, so here we focus on this type of universal correlation and refer to it as the $f - \Lambda$ relation. Given a ρ_c for a specific EOS and a value of β_{QL} , we solve the system of equations (40) and (41) from the center up to the stellar surface for a set of test values ω^2 satisfying the condition (42) at $r=0$. The appropriate frequencies will then be obtained when the boundary condition at the surface (43) is obeyed. This procedure is carried out for a range of central densities, i.e., for all the stellar configurations shown in Fig. 1. As we already mentioned, we are interested in calculating the fundamental mode frequency ω_f . Thus, the dimensionless f -mode oscillation frequencies Ω_f as a function of the tidal deformability Λ are presented in Fig. 4a for several values of the parameters $\tilde{\lambda}$ and β_{QL} . We find the following

empirical expression

$$\Omega_f = \sum_{n=0}^6 d_n (\log_{10} \Lambda)^n, \quad (45)$$

which is represented by the pink curve and the fitting coefficients d_n with their corresponding reduced chi-squared (χ_{red}^2) values are given in Table IV. We observe that the χ_{red}^2 value gets largely (slightly) reduced when adding negative (positive) anisotropy, indicating that anisotropy can enhance this UR.

It was shown that the f -mode also has a connection with the moment of inertia [64]. In that regard, in Fig. 4b we analyze the correlation between the f -mode frequency Ω_f and the normalized moment of inertia \bar{I} , where the numerical data are fitted by the following function

$$\Omega_f = \sum_{n=0}^6 g_n \left(\frac{1}{\bar{I}} \right)^{n/2}. \quad (46)$$

The fitting parameters g_n are listed in Table IV. For the isotropic case (i.e., when $\beta_{\text{QL}}=0$ in the middle panel) we see that this $f - \bar{I}$ relation is insensitive to variations of $\tilde{\lambda}$ with maximum deviations at the 6% level. Nonetheless, this fractional difference decreases slightly when we introduce anisotropy within the IQS, see the specific cases for $\beta_{\text{QL}}=-0.6$ and 0.6 in the side panels. This trend also manifests in the χ_{red}^2 values given in Table IV.

Finally, we will examine the relation between the f -mode frequency and the compactness of anisotropic IQSs. Such a $f - C$ relation is illustrated in Fig. 4c, where the pink curve represents the power series expansion

$$\Omega_f = \sum_{n=0}^4 h_n C^n, \quad (47)$$

with fitting coefficient h_n given in Table IV. Remarkably, for the $f - C$ UR as well as for the other correlations involving the f -mode, the presence of anisotropic pressure (for both positive and negative β_{QL}) decreases the value of χ_{red}^2 with respect to the isotropic scenario. This means that these EOS-independent universal relations become stronger when there is anisotropy within the IQS.

V. SUMMARY AND FINAL REMARKS

In this study, we have systematically explored the various I-Love-C- f universal relations of anisotropic IQSs, with QL anisotropy profile and a general interacting quark matter EOS that subsumes color superconductivity effect, pQCD corrections, bag constant and different phases in a single parameter $\tilde{\lambda}$. We have shown that I-Love-C- f universal relations generally hold, with maximum deviations to the polynomial fit at or below percent levels when varying QM EOS parameter $\tilde{\lambda}$ and anisotropy parameter β_{QL} . With analyses of the reduced χ_{red}^2 values, we find that more positive anisotropy tends to enhance the $\bar{I} - \Lambda$ and $\bar{I} - C$ URs, but weakens the $C - \Lambda$

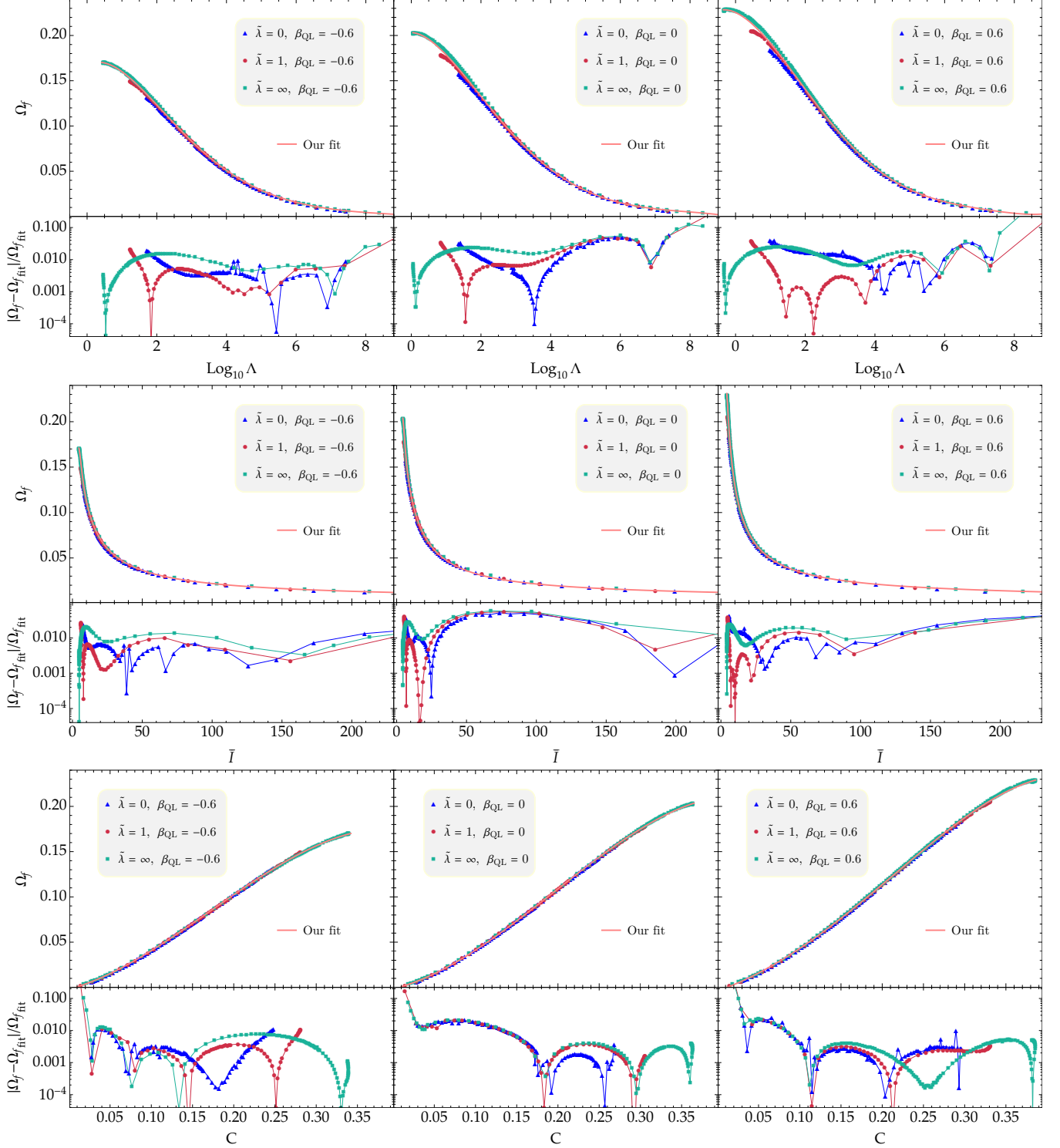


FIG. 4. From top to bottom, dimensional f -mode frequency Ω_f as a function of (a) the tidal deformability Λ , (b) the moment of inertia \bar{I} , (c) the compactness C for anisotropic IQSs. The color and symbol conventions follow those of Fig 2 , where the pink curves represent our fitting functions Eq. (45), Eq. (46), Eq. (47) of corresponding URs, with expansion coefficients listed explicitly in Table IV. The lower panel in each plot displays the relative fractional errors between fits and the numerical results.

TABLE IV. Fitting coefficients for the empirical formulas of the $f - \Lambda$, $f - \bar{I}$ and $f - C$ relations given in Eqs. (45), (46) and (47), respectively. The numerical values for the reduced chi-squared (χ^2_{red}) are shown in the last row.

$f - \Lambda$			$f - \bar{I}$			$f - C$					
β_{QL}	-0.6	0	0.6	β_{QL}	-0.6	0	0.6	β_{QL}	-0.6	0	0.6
$d_0[10^{-1}]$	1.6688	2.0329	2.2532	$g_0[10^{-3}]$	-3.8155	-7.2608	-7.0509	$h_0[10^{-3}]$	-2.0622	-1.5756	-3.9459
$d_1[10^{-2}]$	2.1977	-0.2391	-1.7145	$g_1[10^{-1}]$	2.6599	4.6907	4.0156	$h_1[10^{-1}]$	2.4545	2.1832	3.1808
$d_2[10^{-2}]$	-3.8001	-2.9844	-2.1979	g_2	-1.3375	-5.1309	-3.0898	h_2	2.2344	2.4945	1.5897
$d_3[10^{-3}]$	1.0384	0.8604	0.5514	$g_3[10^1]$	1.9499	4.8932	2.9761	h_3	-4.1448	-3.9546	-0.1437
$d_4[10^{-3}]$	-1.3161	-1.0811	-0.4146	$g_4[10^2]$	-0.8627	-1.9168	-1.0978	h_4	-0.5363	-0.8226	-5.3326
$d_5[10^{-5}]$	8.3270	6.7439	-0.1876	$g_5[10^2]$	1.7164	3.5051	1.9141	--	--	--	--
$d_6[10^{-6}]$	-2.1389	-1.7410	0.9861	$g_6[10^2]$	-1.3045	-2.4521	-1.2975	--	--	--	--
$\chi^2_{\text{red}}[10^{-6}]$	0.9891	8.9843	7.1620	$\chi^2_{\text{red}}[10^{-6}]$	1.5686	9.6502	7.8122	$\chi^2_{\text{red}}[10^{-6}]$	0.2385	5.0862	0.2412

UR. For all the URs involving f -mode frequency, we find that they are enhanced by the inclusion of anisotropy (whether positive or negative).

Note further that in the calculations of f -mode frequencies, we have adopted Cowling approximations since a full GR formalism for determining nonradial pulsations of anisotropic compact stars is still absent in the literature. In addition to the quasi-local ansatz, it is also worthwhile to test other anisotropy models. Moreover, strange quark matter may be localized as solid clusters called strangeons [93–95], which can form strangeon stars that are also highly compact [96–102]. Recently, one of the authors proposed the new possibility of inverted hybrid stars [103, 104]. The anisotropic effect on these new

types of compact stars and related universal relations may also manifest interesting features. We leave these for future studies.

ACKNOWLEDGMENTS

JMZP acknowledges financial support from the PCI program of the Brazilian agency “Conselho Nacional de Desenvolvimento Científico e Tecnológico”–CNPq. C. Zhang is supported by the Jockey Club Institute for Advanced Study at The Hong Kong University of Science and Technology.

-
- [1] A. R. Bodmer, Phys. Rev. D **4**, 1601 (1971).
 [2] E. Witten, Phys. Rev. D **30**, 272 (1984).
 [3] H. Terazawa, *2nd KEK Symposium on Radiation Dosimetry, Tsukuba, Japan, Mar 22-23, 1979*, (1979).
 [4] B. Holdom, J. Ren, and C. Zhang, Phys. Rev. Lett. **120**, 222001 (2018).
 [5] C. Zhang, Phys. Rev. D **101**, 043003 (2020).
 [6] J. Ren and C. Zhang, Phys. Rev. D **102**, 083003 (2020).
 [7] Q. Wang, C. Shi, and H.-S. Zong, Phys. Rev. D **100**, 123003 (2019), [Erratum: Phys. Rev. D **100**, 129903 (2019)].
 [8] C.-J. Xia, S.-S. Xue, R.-X. Xu, and S.-G. Zhou, Phys. Rev. D **101**, 103031 (2020).
 [9] C.-J. Xia, J.-F. Xu, G.-X. Peng, and R.-X. Xu, Phys. Rev. D **106**, 034016 (2022).
 [10] Z. Cao, L.-W. Chen, P.-C. Chu, and Y. Zhou, Phys. Rev. D **106**, 083007 (2022).
 [11] W.-L. Yuan, A. Li, Z. Miao, B. Zuo, and Z. Bai, Phys. Rev. D **105**, 123004 (2022).
 [12] L. Wang, J. Hu, C.-J. Xia, J.-F. Xu, G.-X. Peng, and R.-X. Xu, Galaxies **9**, 70 (2021).
 [13] C.-M. Li, S.-Y. Zuo, Y.-P. Zhao, H.-J. Mu, and Y.-F. Huang, Phys. Rev. D **106**, 116009 (2022).
 [14] T. E. Restrepo, C. Providência, and M. B. Pinto, Phys. Rev. D **107**, 114015 (2023).
 [15] E. Farhi and R. L. Jaffe, Phys. Rev. D **30**, 2379 (1984).
 [16] M. G. Alford, A. Schmitt, K. Rajagopal, and T. Schäfer, Rev. Mod. Phys. **80**, 1455 (2008).
 [17] F. Weber, Prog. Part. Nucl. Phys. **54**, 193 (2005).
 [18] P. Haensel, J. L. Zdunik, and R. Schaeffer, Astron. Astrophys. **160**, 121 (1986).
 [19] C. Alcock, E. Farhi, and A. Olinto, Astrophys. J. **310**, 261 (1986).
 [20] E.-P. Zhou, X. Zhou, and A. Li, Phys. Rev. D **97**, 083015 (2018).
 [21] S. Weissenborn, I. Sagert, G. Pagliara, M. Hempel, and J. Schaffner-Bielich, Astrophys. J. Lett. **740**, L14 (2011).
 [22] R. X. Xu, G. J. Qiao, and B. Zhang, Astrophys. J. Lett. **522**, L109 (1999).
 [23] S.-H. Yang, C.-M. Pi, X.-P. Zheng, and F. Weber, Universe **9**, 202 (2023).
 [24] E. S. Fraga, R. D. Pisarski, and J. Schaffner-Bielich, Phys. Rev. D **63**, 121702 (2001).
 [25] E. S. Fraga, A. Kurkela, and A. Vuorinen, Astrophys. J. Lett. **781**, L25 (2014).
 [26] M. G. Alford, K. Rajagopal, and F. Wilczek, Nucl. Phys. B **537**, 443 (1999).
 [27] K. Rajagopal and F. Wilczek, Phys. Rev. Lett. **86**, 3492 (2001).
 [28] G. Lugones and J. E. Horvath, Phys. Rev. D **66**, 074017 (2002).
 [29] C. Zhang and R. B. Mann, Phys. Rev. D **103**, 063018 (2021).

- [30] C. Zhang, M. Gammon, and R. B. Mann, Phys. Rev. D **104**, 123007 (2021).
- [31] C. Zhang, Phys. Rev. D **104**, 083032 (2021).
- [32] D. Blaschke, E. O. Hanu, and S. Liebing, Phys. Rev. C **105**, 035804 (2022).
- [33] D. Blaschke, U. Shukla, O. Ivanytskyi, and S. Liebing, Phys. Rev. D **107**, 063034 (2023).
- [34] P. T. Oikonomou and C. C. Moustakidis, Phys. Rev. D **108**, 063010 (2023).
- [35] M. Gammon, S. Rourke, and R. B. Mann, Phys. Rev. D **109**, 024026 (2024).
- [36] T. Tangphati, D. J. Gogoi, A. Pradhan, and A. Banerjee, (2023), arXiv:2311.16869 [gr-qc].
- [37] W.-L. Yuan and A. Li, (2023), arXiv:2312.17102 [nucl-th].
- [38] K. Komathiraj and S. D. Maharaj, Int. J. Mod. Phys. D **16**, 1803 (2007).
- [39] T. Harko and M. K. Mak, Chin. J. Astron. Astrophys. **2**, 248 (2002).
- [40] M. Kalam, A. A. Usmani, F. Rahaman, S. M. Hossein, I. Karar, and R. Sharma, Int. J. Theor. Phys. **52**, 3319 (2013).
- [41] J. M. Sunzu, S. D. Maharaj, and S. Ray, Astrophys. Space Sci. **352**, 719 (2014).
- [42] H. Panahi, R. Monadi, and I. Eghdami, Chin. Phys. Lett. **33**, 072601 (2016).
- [43] D. Deb, S. R. Chowdhury, S. Ray, F. Rahaman, and B. K. Guha, Annals Phys. **387**, 239 (2017).
- [44] D. Deb, M. Khlopov, F. Rahaman, S. Ray, and B. K. Guha, Eur. Phys. J. C **78**, 465 (2018).
- [45] J. D. V. Arbañil and M. Malheiro, JCAP **11**, 012 (2016).
- [46] J. D. V. Arbañil, C. V. Flores, C. H. Lenzi, and J. M. Z. Pretel, Phys. Rev. D **107**, 124016 (2023).
- [47] H. C. Das and L. L. Lopes, MNRAS **525**, 3571 (2023).
- [48] L. L. Lopes and H. C. Das, (2023), arXiv:2312.00310 [hep-ph].
- [49] J. M. Z. Pretel, T. Tangphati, A. Banerjee, and A. Pradhan, Phys. Lett. B **848**, 138375 (2024).
- [50] R. L. Bowers and E. P. T. Liang, Astrophys. J. **188**, 657 (1974).
- [51] D. Horvat, S. Ilijic, and A. Marunovic, Class. Quantum Grav. **28**, 025009 (2010).
- [52] L. Herrera and W. Barreto, Phys. Rev. D **88**, 084022 (2013).
- [53] J. M. Z. Pretel, Eur. Phys. J. C **80**, 726 (2020).
- [54] S. R. Mohanty, S. Ghosh, P. Routaray, H. C. Das, and B. Kumar, (2023), arXiv:2305.15724 [nucl-th].
- [55] K. Yagi and N. Yunes, Science **341**, 365 (2013), arXiv:1302.4499 [gr-qc].
- [56] K. Yagi and N. Yunes, Phys. Rev. D **88**, 023009 (2013).
- [57] K. Yagi and N. Yunes, Phys. Rev. D **91**, 123008 (2015).
- [58] K. Yagi and N. Yunes, Phys. Rep. **681**, 1 (2017).
- [59] T. K. Chan, A. P. O. Chan, and P. T. Leung, Phys. Rev. D **93**, 024033 (2016).
- [60] Y. H. Sham, T. K. Chan, L. M. Lin, and P. T. Leung, Astrophys. J. **798**, 121 (2015).
- [61] C.-H. Yeung, L.-M. Lin, N. Andersson, and G. Comer, Universe **7**, 111 (2021).
- [62] A. Maselli, V. Cardoso, V. Ferrari, L. Gualtieri, and P. Pani, Phys. Rev. D **88**, 023007 (2013).
- [63] T. K. Chan, A. P. O. Chan, and P. T. Leung, Phys. Rev. D **91**, 044017 (2015).
- [64] H. K. Lau, P. T. Leung, and L. M. Lin, Astrophys. J. **714**, 1234 (2010).
- [65] T. K. Chan, Y.-H. Sham, P. T. Leung, and L.-M. Lin, Phys. Rev. D **90**, 124023 (2014).
- [66] C. Chirenti, G. H. de Souza, and W. Kastaun, Phys. Rev. D **91**, 044034 (2015).
- [67] T. Zhao and J. M. Lattimer, Phys. Rev. D **106**, 123002 (2022).
- [68] H. C. Das, Phys. Rev. D **106**, 103518 (2022).
- [69] M. Alford, M. Braby, M. W. Paris, and S. Reddy, Astrophys. J. **629**, 969 (2005).
- [70] M. Alford and K. Rajagopal, JHEP **06**, 031 (2002).
- [71] L. Herrera and N. Santos, Phys. Rep. **286**, 53 (1997).
- [72] J. Kumar and P. Bharti, New Astron. Rev. **95**, 101662 (2022).
- [73] M. K. Mak and T. Harko, Proc. R. Soc. Lond. A **459**, 393 (2003).
- [74] H. Abreu, H. Hernández, and L. A. Núñez, Class. Quantum Grav. **24**, 4631 (2007).
- [75] D. D. Doneva and S. S. Yazadjiev, Phys. Rev. D **85**, 124023 (2012).
- [76] A. Rahmansyah, A. Sulaksono, A. B. Wahidin, and A. M. Setiawan, Eur. Phys. J. C **80**, 769 (2020).
- [77] A. Rahmansyah and A. Sulaksono, Phys. Rev. C **104**, 065805 (2021).
- [78] E. J. A. Curi, L. B. Castro, C. V. Flores, and C. H. Lenzi, Eur. Phys. J. C **82**, 527 (2022).
- [79] H. O. Silva *et al.*, Class. Quantum Grav. **32**, 145008 (2015).
- [80] V. Folomeev, Phys. Rev. D **97**, 124009 (2018).
- [81] J. M. Z. Pretel and S. B. Duarte, Class. Quantum Grav. **39**, 155003 (2022).
- [82] T. Tangphati, A. Errehymy, A. Banerjee, and A. Pradhan, J. High Energy Astrophys. **40**, 68 (2023).
- [83] J. Li, B. Yang, Y. Wang, and W. Lin, Phys. Dark Univ. **42**, 101308 (2023).
- [84] J. R. Oppenheimer and G. M. Volkoff, Phys. Rev. **55**, 374 (1939).
- [85] R. C. Tolman, Phys. Rev. **55**, 364 (1939).
- [86] J. B. Hartle, Astrophys. J. **150**, 1005 (1967).
- [87] S. Postnikov, M. Prakash, and J. M. Lattimer, Phys. Rev. D **82**, 024016 (2010).
- [88] T. Hinderer, B. D. Lackey, R. N. Lang, and J. S. Read, Phys. Rev. D **81**, 123016 (2010).
- [89] C. Breu and L. Rezzolla, MNRAS **459**, 646 (2016).
- [90] L. Rezzolla and O. Zanotti, *Relativistic Hydrodynamics*, 1st ed. (Oxford University Press, United Kingdom, 2013).
- [91] L. Lindblom and R. J. Splinter, Astrophys. J. **348**, 198 (1990).
- [92] H. Sotani, N. Yasutake, T. Maruyama, and T. Tatsumi, Phys. Rev. D **83**, 024014 (2011).
- [93] R.-X. Xu, Astrophys. J. Lett. **596**, L59 (2003).
- [94] Z.-Q. Miao, C.-J. Xia, X.-Y. Lai, T. Maruyama, R.-X. Xu, and E.-P. Zhou, Int. J. Mod. Phys. E **31**, 2250037 (2022).
- [95] X. Lai, C. Xia, and R. Xu, Adv. Phys. X **8**, 2137433 (2022).
- [96] X. Lai and R. Xu, MNRAS **398**, 31 (2009).
- [97] X. Lai and R. Xu, J. Phys. Conf. Ser. **861**, 012027 (2017), arXiv:1701.08463 [astro-ph.HE].
- [98] Y. Gao, X.-Y. Lai, L. Shao, and R.-X. Xu, MNRAS **509**, 2758 (2021).
- [99] H.-B. Li, Y. Gao, L. Shao, R.-X. Xu, and R. Xu, MNRAS **516**, 6172 (2022).
- [100] S. Chen, Y. Gao, E. Zhou, and R. Xu, (2023),

- arXiv:2305.19687 [astro-ph.HE].
- [101] C. Zhang, Y. Gao, C.-J. Xia, and R. Xu, Phys. Rev. D **108**, 063002 (2023).
- [102] C. Zhang, Y. Gao, C.-J. Xia, and R. Xu, Phys. Rev. D **108**, 123031 (2023).
- [103] C. Zhang and J. Ren, Phys. Rev. D **108**, 063012 (2023).
- [104] C. Zhang, Y. Luo, H.-b. Li, L. Shao, and R. Xu, (2023), arXiv:2306.08234 [astro-ph.HE].